Am J Physiol Renal Physiol 310: F1089–F1102, 2016.
First published February 17, 2016; doi:10.1152/ajprenal.00605.2015.

Mechanism of increased clearance of glycated albumin by proximal tubule cells

Mark C. Wagner,[1] Jered Myslinski,[1] Shiv Pratap,[4] Brittany Flores,[1] George Rhodes,[1] Silvia B. Campos-Bilderback,[1] Ruben M. Sandoval,[1] Sudhanshu Kumar,[1] Monika Patel,[1] Ashish,[4] and Bruce A. Molitoris[1,2,3]

[1]*Nephrology Division, Department of Medicine, Indiana University School of Medicine, Indianapolis, Indiana; and* [2]*Department of Cellular and Integrative Physiology, Indiana University School of Medicine, Indianapolis, Indiana;* [3]*Roudebush Veterans Affairs Medical Center, Indianapolis, Indiana; and* [4]*The Council of Scientific and Industrial Research Institute of Microbial Technology, Chandigarh, India*

Submitted 7 January 2016; accepted in final form 10 February 2016

Wagner MC, Myslinski J, Pratap S, Flores B, Rhodes G, Campos-Bilderback SB, Sandoval R, Kumar S, Patel M, Ashish, Molitoris BA. Mechanism of increased clearance of glycated albumin by proximal tubule cells. *Am J Physiol Renal Physiol* 310: F1089–F1102, 2016. First published February 17, 2016; doi:10.1152/ajprenal.00605.2015.—Serum albumin is the most abundant plasma protein and has a long half-life due to neonatal Fc receptor (FcRn)-mediated transcytosis by many cell types, including proximal tubule cells of the kidney. Albumin also interacts with, and is modified by, many small and large molecules. Therefore, the focus of the present study was to address the impact of specific known biological albumin modifications on albumin-FcRn binding and cellular handling. Binding at pH 6.0 and 7.4 was performed since FcRn binds albumin strongly at acidic pH and releases it after transcytosis at physiological pH. Equilibrium dissociation constants were measured using microscale thermophoresis. Since studies have shown that glycated albumin is excreted in the urine at a higher rate than unmodified albumin, we studied glucose and methylgloxal modified albumins (21 days). All had reduced affinity to FcRn at pH 6.0, suggesting these albumins would not be returned to the circulation via the transcytotic pathway. To address why modified albumin has reduced affinity, we analyzed the structure of the modified albumins using small-angle X-ray scattering. This analysis showed significant structural changes occurring to albumin with glycation, particularly in the FcRn-binding region, which could explain the reduced affinity to FcRn. These results offer an explanation for enhanced proximal tubule-mediated sorting and clearance of abnormal albumins.

albuminuria; glycation; diabetes; cell biology and structure; proximal tubule; neonatal Fc receptor

ALBUMIN is the most abundant soluble protein in the body and the major protein in plasma (39). It has been extensively studied and has many important functions, including colloid osmotic pressure, as an antioxidant, transport of endogenous and exogenous compounds, and pH buffering capacity (44, 47). It is a protein of ~66 kDa, composed of three homologous domains that interact with a variety of ligands, fatty acids, drugs, proteins, and various small molecules, such as sugars. Some of these interactions alter its physical properties and are known to increase in certain disease states. In particular, glucosylated proteins derived from glucose and dicarbonyl α-oxaldehyde methylglyoxal (MGO) incubations are closely associated with hyperglycemia, poor control of diabetes, and increased susceptibility to diabetic complications, including nephropathy (8, 45, 48). These modifications are known to result in albuminuria; however, the mechanism(s) responsible for this is still being discovered.

The normal half-life of albumin is ~21 days in human and ~3 days in rats, and it is dependent on its interaction with the neonatal Fc receptor (FcRn) (27). FcRn is a heterodimeric integral membrane protein composed of an α-chain of the nonclassical major histocompatibility complex class I family and β_2-microglobulin (69). It contains distinct and noninteractive binding sites for its two known ligands (IgG and albumin), and its affinity for each is increased >100-fold in an acidic environment (10). The FcRn-IgG interaction has been studied extensively, and multiple studies have supported increased ligand binding in endosomes that prevents ligand targeting to lysosomes followed by ligand transcytosis and subsequent extracellular release (18, 21, 37, 42). More recent studies have documented the presence of FcRn in the brush border of proximal tubule cells (20), direct visualization of albumin transcytosis in proximal tubule cells intravitally (55), and molecular evidence for an active role of FcRn in proximal tubule albumin transcytosis (56, 68). Using fluorescently tagged albumin with intravital microscopy in Munich-Wistar-Fromter (MWF) rat kidneys has enabled real-time visualization and analysis of glomerular albumin filtration and proximal tubule reabsorption and trafficking (14, 55). Thereafter, endothelial transcytosis, mediated by FcRn, returns albumin to the circulation.

Characterizing the biochemical interaction between albumin and FcRn is essential to fully understand how albumin modifications impact urinary loss of albumin by affecting either binding and/or trafficking. Multiple studies using several animal models have shown that glycated albumin is handled differently compared with unmodified albumin (17, 29, 30). We recently showed in a diabetic model that reduced albumin uptake occurred by proximal tubules although no change in the of fluorophore-labeled albumin was measured (50). We also confirmed that the majority of albumin in urine is present as albumin-derived fragments of 300–500 Da (50). What is unknown is whether glycated albumin binding to albumin receptors is altered and could explain this observation. Microscale thermophoresis (MST) has proven to be a powerful method to address protein-protein interactions (60) and was used to evaluate albumin-FcRn interactions. In addition, previous studies have documented secondary structure changes in albumin when modified (24, 48, 61). To extend these findings to modified albumins of physiological importance, small-angle X-ray scattering (SAXS) was conducted to determine if there was a correlation between global shape changes and the observed altered binding. Both analyses were done in solution to mimic the possible changes occurring in vivo. In addition, we

Address for reprint requests and other correspondence: B. A. Molitoris, Indiana Univ. School of Medicine, Nephrology Division, 950 W. Walnut St., R2-202, Indianapolis, IN 46202 (e-mail: bmolitor@iu.edu).

evaluated the glomerular filtration of glycated albumin and proximal tubule uptake to provide a more complete picture of its kidney dynamics.

MATERIALS AND METHODS

Two-photon microscopy. Imaging was conducted using an Olympus FV1000 microscope adapted for two-photon microscopy with high-sensitivity gallium arsenide nondescanned 12-bit detectors with animal preparations, as previously described elsewhere (54, 55). Animals were anesthetized with pentobarbital sodium (50 mg/ml). A jugular venous line was used to introduce fluorescent albumin. As previously described, animal body temperature, saline bath temperature in the dish, and heart rate and blood pressure (90 mmHg average) were measured using LabChart 6 (AD Instruments, Colorado Springs, CO) (54). All rats had normal body temperature and blood pressure, and hydration was maintained by saline infusion. Glomerular sieving coefficients (GSCs) were determined using our previously published method (55). Briefly, *z*-stack images of the glomerulus before fluorescent rat serum albumin (RSA) infusion were collected to enable background fluorescent levels of the Bowman's space and glomerular capillaries to be quantified. These values were subtracted from the same region after the fluorescent albumin infusion. Quantification of intensity values was performed using Metamorph (Molecuar Devices) or ImageJ. Graphing and statistical analyses were performed using Microsoft Excel (Redmond, CA), KaleidaGraph (Synergy Software, Reading, PA), and GraphPad Prism 5 (La Jolla, CA).

Proteins. Soluble rat FcRn (srFcRn) and soluble human FcRn (shFcRn) were purified from Chinese hamster ovary cell lines generously provided by Dr. Pamela Bjorkman (Howard Hughes Medical Institute at California Institute of Technology) (16, 75). Cells were grown in custom α-MEM (Lonza) plus 5% dialyzed FBS, penicillin, streptomycin, and methionine sulfoximine as previously described. srFcRn was purified from the culture supernatant using pH-dependent binding to the rat IgG agarose column as described previously (16). shFcRn was also purified from the culture supernatant using pH-dependent binding to the human IgG agarose column. Removal of bound BSA required further purification using an anion exchange column as previously described (75). Albumins were purchased from Sigma (bovine, mouse, and rat), Equitech-Bio (porcine, rabbit, and sheep), and Albumin BioScience (human). IgGs were purchased from Equitech-Bio (bovine, human, mouse, and rat) and Rockland Immunochemicals (rabbit). DQ red BSA was purchased from Life Technologies.

Modified albumin and FcRn. Rat and human albumin were glycated using glucose or methylgloxal as previously described (24). Briefly, albumin was incubated at 37°C for 21 days in the presence of glucose (20, 200, and 500 mM) or methyglgloxal (1 and 5 mM). Conjugation of a fluorescent tag to albumin and FcRn was done using fluorescent dyes [NT-red and NT-blue from Nanotemper Technologies; Alexa 647, Alexa 568, Alexa 488, Texas red (TR), FITC, and TR-X from Life Technologies; CF594 was a free sample from Biotium] according to the manufacturers' protocols. The dye-to-protein molar ratio was varied to achieve the conjugation desired, and free dye was separated by desalting and/or dialysis.

MST. MST was used to characterize binding affinity between purified FcRns and albumin (26, 60). Binding assays were performed with the Monolith NT.115 MST device using standard capillaries (NanoTemper Technologies, Munich, Germany). Measurements were performed at 25°C in 67 mM $NaPO_4$ buffer, 150 mM NaCl, and 0.05% Tween 20 at pH 6.0 or 7.4. The infared laser power was between 20 and 60%, and 40–70% LED power was used. A laser on time of 30 s and a laser off time of 5 s were used. Data from a minimum of three replicate binding assays were analyzed using Nanotemper analysis and GraphPad Prism software. Final data normalization and curve fitting were performed with GraphPad Prism. It is important to note that this instrument requires a fluorescent tag be placed on either the receptor or ligand. Note that the weak binding measurements are approximate and the equilibrium dissociation constant (K_D) in this case is listed as >100 μM.

SAXS data acquisition. Lyophilized samples of rFcRn, RSA, and its glycated versions [RSA modified with 20, 200, and 500 mM glucose (RSA_20G, RSA_200G, and RSA_500G, respectively)] were dissolved in 67 mM sodium phosphate buffer, 150 mM NaCl, 1 mM NaN_3, and 0.05% Tween 20. Sodium phosphate buffer was used for pH 6–8, whereas 10 mM sodium acetate buffer was used for pH 4 and 5. The purity of the samples was ascertained by single bands near the expected migration position in 12% SDS-PAGE relative to standard markers (Thermo Scientific), and their intact masses were obtained by matrix-assisted laser desorption/ionization-time of flight (TOF) mass spectrometry (AB-Sciex TOF/TOF 72092). Microdialysis was used to exchange buffer pH as required, and the last dialysis buffer was used as the matched buffer for SAXS experiments. Binding experiments were done at a 1:1 stochiometric ratio of rFcRn and RSA. Before SAXS data collection, samples were centrifuged at 60,000 *g* using a Beckman TLA 120.2 for 1 h to remove any aggregates. Data were collected using a SAXSpace instrument with a sealed tube source (Anton Paar, Graz, Austria). All experiments were done using line collimation, and scattered X-rays were recorded on a one-dimensional CMOS Mythen detector (Dectris, Baden, Switzerland). In each case, 60-μl samples and their matched buffer were exposed for 1 h at 20°C in the same thermostated quartz capillary with a 1-mm diameter (63). The capillary was washed with water, 1 M NaOH, and isopropanol before and after each data collection. SAXStreat software was used to convert scattering data as intensity points at each pixel and calibrate the position of the primary beam. Data were further processed using SAXSquant software to obtain intensity (I) as a function of Q [where $Q = 4\pi(\sin\theta)/\lambda$, where θ is the angle and λ is wavelength], i.e., I(Q), for all samples and buffers. Then, contribution of buffer was subtracted. In addition, the Porod constant (*C*) was calculated and subtracted from sample I(Q) to obtain an intensity profile, where the scattering of the particle decays as a function of Q^{-3}. I(Q) profiles in reciprocal space were analyzed by generalized indirect Fourier transform software to *1*) desmear the data from line collimation and represent a true point collimation and *2*) estimate the pairwise distribution function of interatomic vectors [P(r)] profiles of interatomic scattering vectors contributing to the obtained SAXS I(Q) profiles, as previously described (63).

SAXS data analysis and modeling. Desmeared I(Q) files were analyzed using Guinier analyses presuming globular- and rod-like scattering shapes of the scattering particles, which yielded the radius of gyration (R_g) and radius of cross-section (R_c), respectively. These analyses were done using the AUTORG program in the ATSAS 2.6 suite of programs (28). Kratky plots [$I(Q) \times Q^2$ vs. Q] of each data set were prepared to examine the nature of scattering protein in the solution. Having confirmed globular scattering profiles, the AUTOGNOM program (66) was used to perform indirect Fourier transformation of the scattering data to obtain P(r). During the transformation, the probablity of finding a pairwise vector equal to 0 Å and the maximum linear dimension (D_{max}) was considered to be zero. To visualize the predominant solution shape of rFcRn, RSA, and its glycated versions, for each data set, 10 independent uniform density models were generated using Dammin software (65, 67). These models were compared with each other using the DAMCLUST program (40). As described below, the models with the best correlation between the experimental data and theoretical SAXS profile of the model were used for comparison with crystal structures and analysis. The CRYSOL program was used to compute the theoretical SAXS profile of the final residue level models and compare it with experimental data (64).

Isoelectric focusing. Novex pH 3–10 isoelectric focusing (IEF) protein gels and SERVA Liquid Mix IEF Marker pI 3.5–10.7 were purchased from Life Technologies. Three to five micrograms of each protein sample was used, and gels were run according to the manu-

facturer's protocol, fixed with 12% TCA, and stained with Pierce GelCode Blue (Fisher Scientific).

Rat clearance experiments. Male Sprague-Dawley rats (180–220 g) were purchased from Harlan and acclimated for 4 days. Blood and urine were obtained to establish baseline values. Rats were anesthetized with isofluorane, and 1.5 mg of fluorescently tagged RSA were injected intraperitoneally or by tail vein. Blood was collected postinjection at 15 min, 2 h, and 24 h. Each tagged albumin was evaluated in four rats unless stated otherwise in the figures. Blood was collected in heparinized tubes, spun, and assayed for fluorescence using a Molecular Devices SpectraMax M5 plate reader. The 15-min collection time point was set to 100%, and the decrease in fluorescence followed at 2 and 24 h. All experiments followed National Institutes of Health *Guide for the Care and use of Animals* guidelines and were approved by the Animal Care and Use Committee of the Indiana University School of Medicine. All rats had normal blood and urine creatinine and protein values before infusion and at the end of the study.

RESULTS

Two-photon imaging shows no GSC increase and normal proximal tubule uptake of glycated albumin. To evaluate the glomerular filtration of glycated albumin and proximal tubule uptake, healthy MWF rats were infused with 1–3 mg of fluorophore conjugated glycated albumin (either glucose or methylglioxal modified). The GSC was 0.014 ± 0.003 for 500 mM glucose-modified albumin and 0.014 ± 0.010 for 1 mM MGO-modified albumin. Note that these GSCs are consistent with our previously published values for normal albumin in these rats: 0.010 ± 0.001 (55). To evaluate albumin uptake, proximal tubules were examined after infusion. Figure 1*A* shows the uptake (~60 min after infusion) of MGO-modified albumin in proximal tubules, whereas Fig. 1*B* shows both low- and high-power views of glucose-modified albumin present in proximal tubules after infusion. Each image is presented in black and white as well as pseudocolor. Note that for both modified albumins, the uptake pattern was indistinguishable from our previous reports with unmodified albumin (50, 51, 55). These results are consistent with glycated albumin being filtered and taken up by proximal tubules normally, thus implicating a proximal tubule handling alteration.

MST characterization of rat FcRn binding to albumin and IgG from multiple species. Our overall focus was to define the mechanisms mediating albumin handling in the kidney. The MWF rat model enabled us to quantify both glomerular filtration and proximal tubule uptake of albumin using two-photon intravital microscopy. This method also requires the attachment of a fluorescent probe to either the ligand, albumin, or receptor (FcRn) being studied. Since FcRn is a key albumin receptor responsible for albumin transcytosis, and thus the albumin salvage pathway in the proximal tubule, our initial experiments quantified K_D using MST. Figure 2, *A* and *B*,

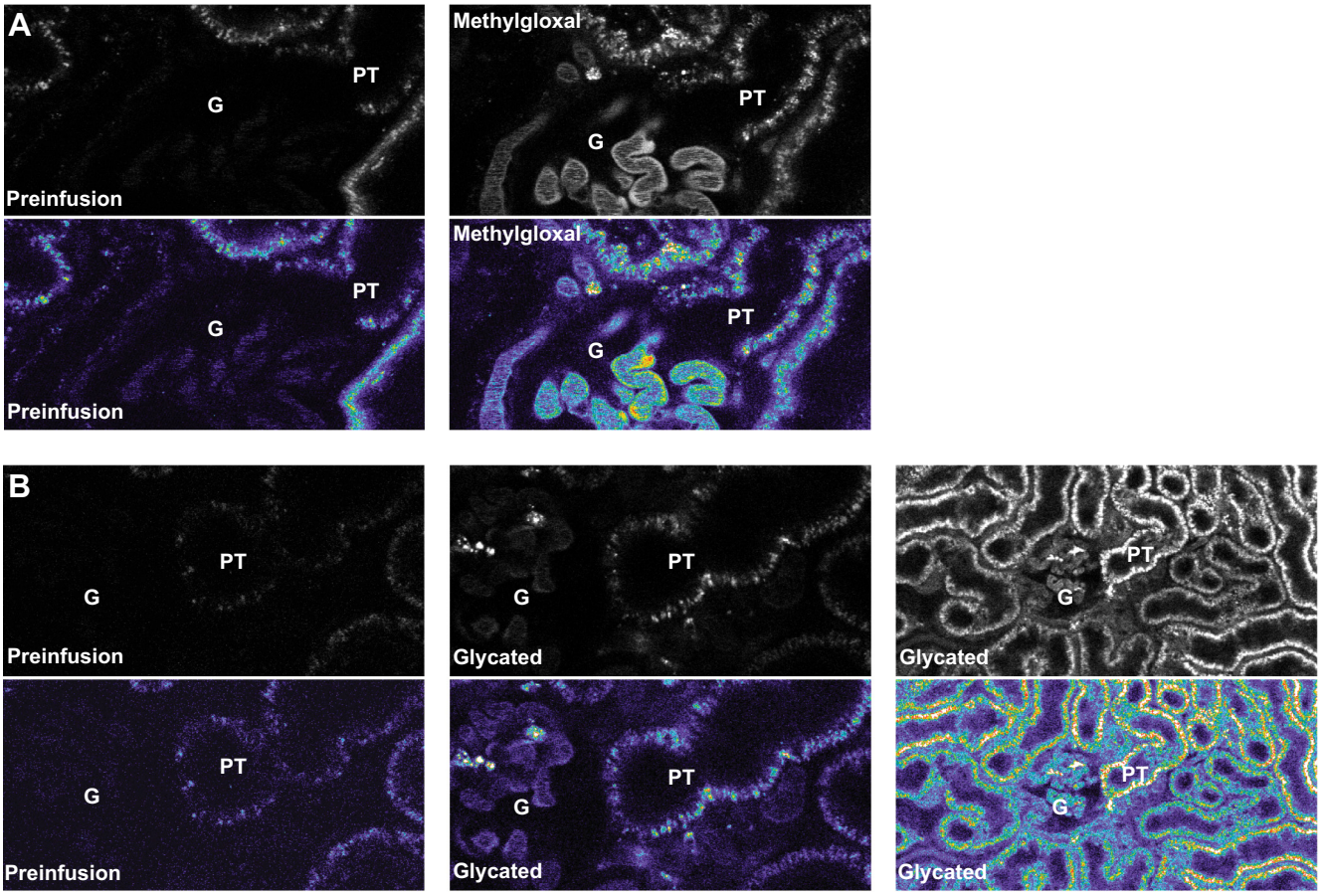

Fig. 1. Proximal tubule uptake of glycated albumin is normal when infused into healthy rats. *A*: representative two-photon images of rats infused with methylgloxal-modified albumin. *B*: representative two-photon images of rats infused with glucose-modified albumin. Each image is presented in both black and white as well as pseudocolor and shows significant proximal tubule (PL) uptake after infusion. G, glomerulus.

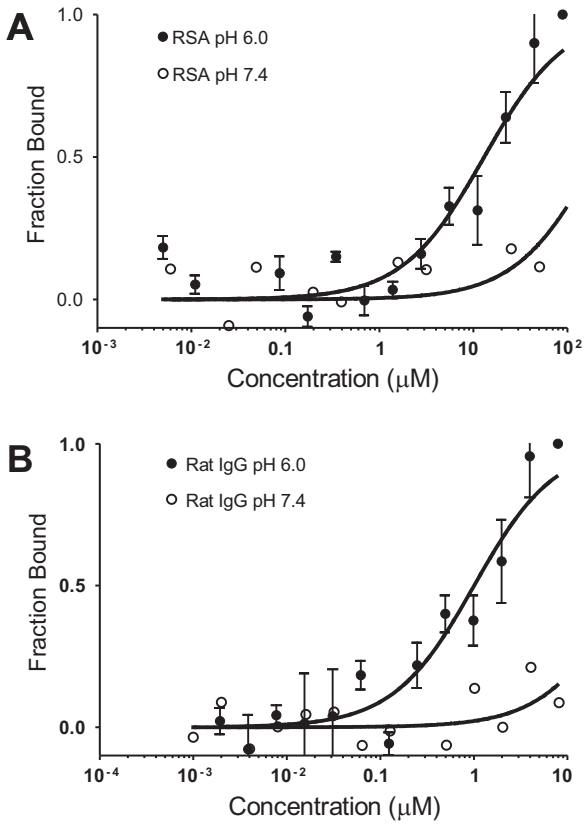

Fig. 2. Microscale thermophoresis (MST) confirming a pH-sensitive interaction between the neonatal Fc receptor (FcRn) and both albumin and IgG. MST was used to characterize the interaction between FcRn and rat serum albumin (RSA; *A*) and between FcRn and IgG at pH 6.0 and 7.4 (*B*). Equal amounts of fluorescently labeled (NT-647) rat (r)FcRn were titrated with unlabeled RSA or IgG. Graphs are presented as fraction bound versus log of the concentration; $n = 3$. K_D values of 10 and 1 μM were calculated for FcRn versus albumin and IgG, respectively, at pH 6.0.

shows the pH-sensitive binding of srFcRn to albumin and IgG, respectively. The graphs are presented as the fraction bound versus log of the concentration that gave a K_D of 11.6 μM for albumin and 1.8 μM for IgG at pH 6.0 with both being >100 μM at pH 7.4. These measured binding constants are consistent with previous studies (10, 53).

Multiple animal studies have used albumin from different species interchangeably, but recent evidence has identified considerable species differences for FcRn binding to albumin and IgG (2, 3, 5, 10, 11, 15, 22, 34, 36, 38, 72, 75, 76). To extend these studies and define more completely the interactions of rFcRn, we compared albumins from several different species and IgGs against srFcRn using MST analysis. Figure 3*A* shows the binding curves for albumins at pH 6.0. srFcRn bound rabbit albumin with comparable affinity to rat albumin at pH 6.0, whereas bovine, human, mouse, porcine, and sheep albumin had K_D values of >100 μM. Figure 3*B* shows the binding curves for IgGs at pH 6.0. srFcRn had a slighty stronger affinity to rabbit and human IgG than rat and bovine IgG, with mouse IgG having very weak binding. Table 1 shows our binding results and summarizes those of other laboratories who examined FcRn interactions with albumin and IgG. While not complete, these studies do indicate it is best to use species-specific ligand FcRn combinations since significant differences between species can be present.

Glycation of albumin reduces affinity to FcRn. Glycated albumin has been shown to be preferentially excreted in the urine (17, 29, 30). To evaluate whether decreased affinity for FcRn contributed to increased glycated albuminuria, we used MST to quantify K_D values between modified albumins and FcRn. Albumin was glycated with three concentrations of glucose (20, 200, and 500 mM) for 21 days. Figure 4*A* shows the binding curves for glucose-modified rat albumin, and Fig. 4*C* shows human albumin at pH 6.0. For both rat and human FcRn, K_D increased with the level of glycation, indicating that glycation of albumin does reduce its interaction with FcRn in a dose-dependent fashion. Methylglloxal, which is also increased in diabetic patients, also led to a reduction in FcRn binding to albumin. Albumin was incubated with 1 or 5 mM methylglloxal for 21 days. The MST binding curves show that both rat (Fig. 4*B*) and human (Fig. 4*D*) methylglloxal-modified albumin had reduced binding to FcRn at pH 6.0. Table 2 shows the albumin-FcRn K_D values for these modified albumins at pH 6.0 and 7.4. These data indicate that binding of albumin to FcRn is reduced by albumin modifications that occur clinically.

SAXS data analysis from albumins with or without FcRn. Intact molecular masses of RSA, RSA_20G, RSA_200G, and RSA_500G were observed to be 65.87, 67.46, 67.94, and 69.57

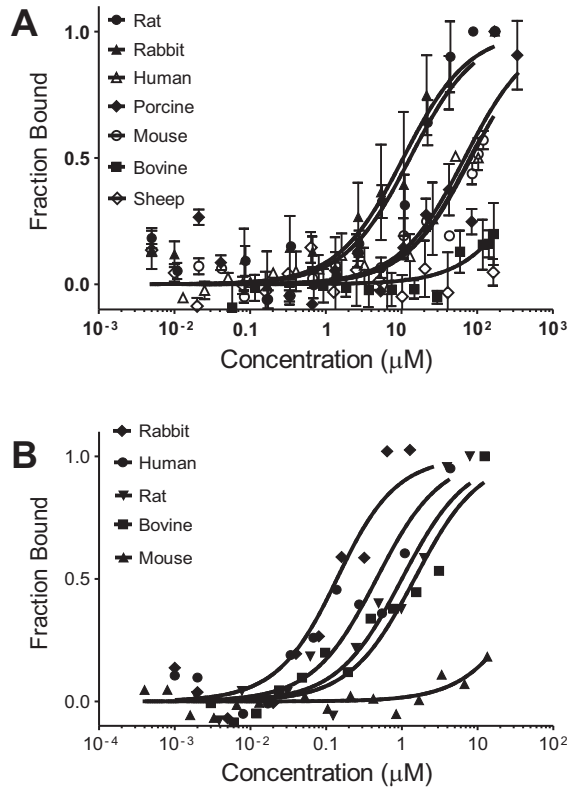

Fig. 3. MST documenting species differences in binding between rat FcRn and albumins and IgG molecules. MST was used to evaluate rabbit, human, bovine, and mouse albumin (*A*) and IgG (*B*) binding to rFcRn at pH 6.0. Equal amounts of fluorescently labeled (NT-647) rFcRn were titrated with unlabeled albumin or IgG. Graphs are presented as fraction bound versus log of the concentration. Rabbit albumin had a K_D value of 11.8 μM, whereas all other albumins had K_D values of >100 μM. In contrast, rabbit IgG (K_D: 0.19 μM) and human IgG (K_D: 0.63 μM) had a slightly stronger affinity with rFcRn than rat IgG, whereas bovine IgG had a K_D value of 1.5 μM and mouse IgG had a K_D value of >100 μM. Interestingly, bovine IgG did not show pH-sensitive binding and retained a strong K_D value of 1.2 μM at pH 7.4 ($n = 3$; see Table 1).

Table 1. *Assessment of rFcRn binding to albumins and IgGs using MST analysis*

Ligand	rFcRn pH 6 K_D, μM	Human FcRn pH 6 K_D, μM	Mouse FcRn pH 6 K_D, μM
		Albumins	
Rat	11.6*	~1.1 (34)	SB (34)
Rabbit	11.8*		
Human	>100*	4.6 (22); 5.2 (38)	~86 (72)
Human	WB (34, 36)	1.1 (34)	WB (34)
Porcine	>100*	>50*	
Mouse	>100*	0.8 (72)	9.3 (72); SB (34)
Bovine	>100*; WB (36)		
Sheep	>100*		
Rhesus	WB (34)		
		IgGs	
Rat	1.8*		~0.45 (11)
Rat IgG2a	0.014 (75)	NB (75)	
Rabbit	0.19*	SB (76)	SB (76)
Human	0.63*	0.70 (2)	0.265 (10)
	0.03 (75)	0.09 (75)	
Human	0.50 (3)	2.35 (10)	1.2 (72)
Human IgG1		0.63 (15)	0.082 (15)
Bovine	1.5*	WB (76)	SB (76)
Mouse	>100*	WB (76)	~0.01 (72)
Mouse IgG1		>50 (15)	0.75 (15)
Mouse IgG2a	0.019 (75)	NB (75)	0.025 (75)
Rat and mouse IgGs	~0.05 (5)		

Data shown are from the indicated references. *Data from the present study. FcRn, neonatal Fc receptor; rFcRn, rat FcRn; MST, microscale thermophoresis; WB, weak binding; SB, strong binding; NB, no binding.

kDa, respectively. This indicated that upon chemical modification, on average, 8.8 (close integer: 9), 11.5 (close integer: 11), and 20.5 (close integer: 20) molecules of sugar got attached to RSA, respectively. The I(Q) profiles, as plotted in log I(Q) versus log Q, indicated lack of aggregation or interparticulate nature in the samples (Fig. 5*A*). The linear nature of the Guinier analysis of the data sets, presuming globular scattering shape, further confirmed the monodispersity of the samples (Fig. 5*A*, *insets*). The slope of the fit provided R_g values of RSA_20G, RSA_200G, and RSA_500G to be 2.9, 3.5, 3.6, and 4.0 nm, respectively. Similarly, presuming a rod-like scattering shape, R_c values of the proteins were found to be 1.8, 1.9, 2.0, and 2.0 nm, respectively. From these values, the persistent lengths [L; where $L = 12(R_g^2 - R_c^2)$] of the scattering shape of the proteins were estimated to be 8, 10, 10, and 12 nm, respectively. Peak-like profiles of the Kratky plots of the SAXS I(Q) values from unliganded albumins confirmed that these proteins are globular in solution (Fig. 5*B*). P(r) analysis brought forth that D_{max} values of RSA, RSA_20G, RSA_200G, and RSA_500G were 8.3, 10.8, 10.2 and 12.4 and and R_g values were 2.9, 3.5, 3.6, and 4.1 nm, respectively (Fig. 5*C* and Table 3). Importantly, molecular weight estimations of RSA, RSA_20G, RSA_200G, and RSA_500G, based on volume correlation, were found to be 66.38, 72.26, 74.55, and 71.63 kDa, respectively, indicating that all these albumins remained mostly monomer, even after glycation (46).

Guinier analysis of the SAXS data of rFcRn (complexed with β_2-microglobulin) suggested its R_g, R_c, and L to be 3.2, 1.8, and 9 nm, respectively (Fig. 5*D*). Kratky analysis supported the globular scattering profile of the molecules in solutions (Fig. 4*E*). P(r) analysis suggested that the shape of rFcRn at pH 6 was characterized by D_{max} and R_g values of 10.3 and 3.2 nm, respectively (Fig. 5*F*). Furthermore, the volume of correlation suggested its mass to be 84.17 kDa, a value very close to its expected mass of its dimer, 86 kDa (73). This sample of rFcRn was mixed with the nonglycated and glycated albumins at a 1:1 molar ratio, and their SAXS data were acquired. Guinier analysis of data sets confirmed the monodispersity of the samples, and the slope of the fit presuming globular shape provided R_g values of rFcRn complexed with RSA, RSA_20G, RSA_200G, and RSA_500G of 3.5, 3.7, 3.8, and 4.5 nm, respectively. Presuming a rod-like scattering shape provided R_c values of 1.9, 1.8, 1.6 and 1.4, nm for the proteins. Based on these values, L values of the predominant scattering species in the mixtures were estimated to be 10, 11, 12, and 15 nm, respectively. Furthermore, Kratky analysis supported globular shapes of complexes, but relatively higher inherent motion was observed compared with the unliganded proteins (Fig. 5*E* and Table 3). P(r) analysis suggested D_{max} values of the 1:1 molar mixture of rFcRn with RSA, RSA_20G, RSA_200G, and RSA_500G to be 12.2, 14.3, 13.8 and 16 and R_g values of 3.5, 3.8, 4.0 and 4.8 nm, respectively (Fig. 5*F* and Table 3). Furthermore, molecular weight estimations of the predominant scattering species in the mixtures were estimated to be 109.48, 112.36, 115.67, and 114.63 kDa, respectively. These data upheld the 1:1 stoichiometry of the proteins in the complexes or, in other words, one molecule of rFcRn (complexed with β_2-microglobin) binds to one molecule of RSA despite glycation. Note the scattering data profile is dependent on the molecular mass and relative abundance of each scattering species; thus, even in instances of partial binding, the SAXS data will be dominated by the complex.

Global shapes of RSAs with or without rFcRn. Solution shapes of the albumins were computed using the constraints offered in the SAXS data profiles. Shape thus restored for unmodified RSA matched well with the crystal structure of monomeric RSA (Protein Database ID 4K2C). Automated alignment of inertial axes of the SAXS data-based model and crystal structure confirmed the similarity between the two results (Fig. 6). The crystal structure helped in realizing how the volumes of the three domains of albumin packed inside the overall envelope. Interestingly, shapes restored for RSA_20G, RSA_200G, and RSA_500G suggested that the domains of the proteins appeared to open up with increase in glycation. In the

Table 2. *Assessment of FcRn binding to glucose- and methylglyoxal-modified albumin*

Ligand	pH 6 K_D, μM	pH 7.4 K_D, μM
	Rat albumins against rFcRn	
Unmodified	11.6	>100
20 mM Glucose	78	>100
200 mM Glucose	>100	>100
500 mM Glucose	>100	>100
1 mM Methylglyoxal	>100	>100
5 mM Methylglyoxal	>100	>100
	Human albumins against human FcRn	
Unmodified	7.5	>100
20 mM Glucose	36	ND
200 mM Glucose	>100	ND
500 mM Glucose	>100	ND
1 mM Methylglyoxal	42	ND
5 mM Methylglyoxal	>100	ND

ND, not determined.

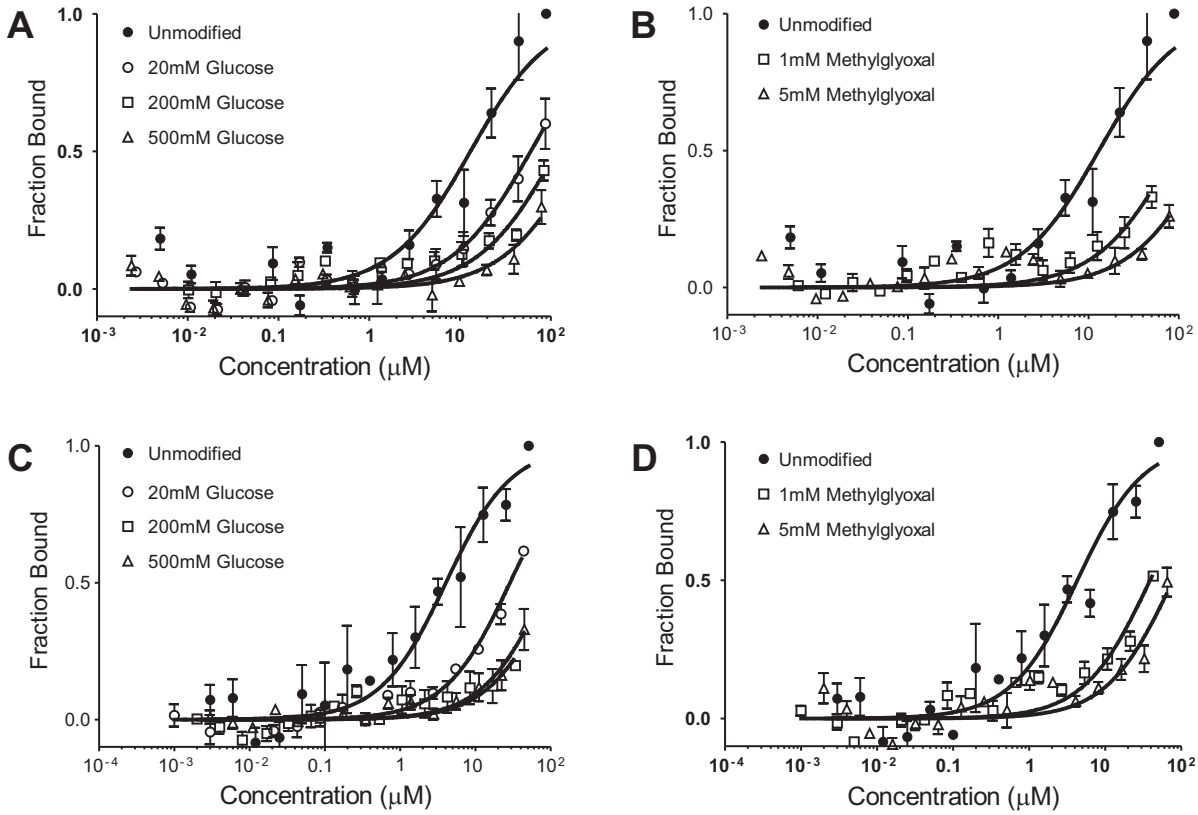

Fig. 4. MST showing that glycated albumin has reduced binding to FcRn. MST was used to determine binding affinity between rFcRn and human FcRn and glycated albumins at pH 6.0. Equal amounts of fluorescently labeled (NT-647) rFcRn were titrated with unlabeled modified albumin. Graphs are presented as fraction bound versus log of the concentration. *A*: reduced K_D values between rFcRn and glucose-modified rat albumin. *B*: comparable reduction in binding when rat albumin was modified with methylglyoxal. Human FcRn showed similar decreases in affinity to glucose-modified (*C*) or methylglyoxal-modified (*D*) human albumin. K_D values at pH 7.4 were >100 μM for all modified albumins ($n = 3$; see Table 2).

absence of the crystal structure of glycated albumin, these shapes could not be compared with high-resolution structures.

The global shape of the 1:1 complex of RSA-rFcRn was compared with the complex of the same proteins by aligning the inertial axes in an automated manner (Fig. 7). The overlay confirmed that the two proteins remained tightly bound in solution, as seen in the crystal structure. Interestingly, the shapes of 1:1 complexes of rFcRn with glycated RSAs showed that the complexes seemed to extend out in one direction.

Shape of rFcRn as a function of buffer pH. SAXS data were collected for rFcRn in buffer with varying pH to determine if any shape changes occur as a function of pH. Guinier analysis suggested R_g and R_c values at pH 4, 5, 6, 7, and 8 to be 3.5, 3, 3.2, 3.1, and 3.5 nm and 2.1, 1.9, 1.8, 1.7, and 2 nm, respectively (Table 3). Based on these values, the estimated persistence length of rFcRn/β_2-microglobulin was estimated to be 9.7, 8.0, 9.2, 9.0, and 9.9 nm at pH 4, 5, 6, 7, and 8, respectively. Kratky analysis of the variable pH data sets supported globular profiles of molecules in solution. Furthermore, P(r) analysis suggested D_{max} values for pH 4, 5, 6, 7, and 8 to be 10.8, 10.4, 10.6, 10.8 and 12 nm and and R_g values to be 3.5, 3.1, 3.3, 3.2 and 3.6 nm, respectively. SAXS data analysis indicated that the rFcRn/β_2-microglobulin complex appears to be most compact at pH 6 and open up on increasing or decreasing buffer pH. Additionally, molecular masses of the predominant species in the mixtures were estimated to be 81.79, 80.61, 84.24, 83.26, and 88.48 kDa, respectively.

Shapes of rFcRn/β_2-microglobin in different pHs were restored from their SAXS data profiles (Fig. 4, *G–I*). The dummy atom, a model computed for the rFcRn/β_2-microglobin complex, was compared with the crystal structure 3FRU, which showed that the solution shape matched the complex in crystalline state and is a dimer of the heteromeric complex (Fig. 8). The shape seemed to change little as the buffer was changed from pH 6 to 4, but at pH 8, the complex appeared to open up or the sample had partial aggregation or both. Probably, these changes compromised the ability of FcRn to bind albumins at physiological or high pHs.

RSA charge is altered by glycation or tag addition. IEF gels were used to determine the pI of modified albumins. Figure 9 shows a Coomassie blue-stained IEF gel (3–10) of unlabeled albumin and albumin labeled with multiple different fluorescent tags conjugated at different dye to albumin ratios. A commercially available TR-labeled BSA (DQ) is also shown along with the glycated RSA that was examined in earlier binding experiments. Note that Alexa 488, Alexa 568, and FITC all make RSA more anionic, whereas DQ BSA separated into a diverse set of protein bands. The shift to a more anionic albumin also occurs with glycation. Higher concentrations of glucose and MGO showed the greatest shift. Finally, TR, CF-594, and Alexa 647 caused little if any alteration in the pI of RSA when conjugated to RSA. These data indicate that both fluorescent tag conjugation and glycation of albumin can make

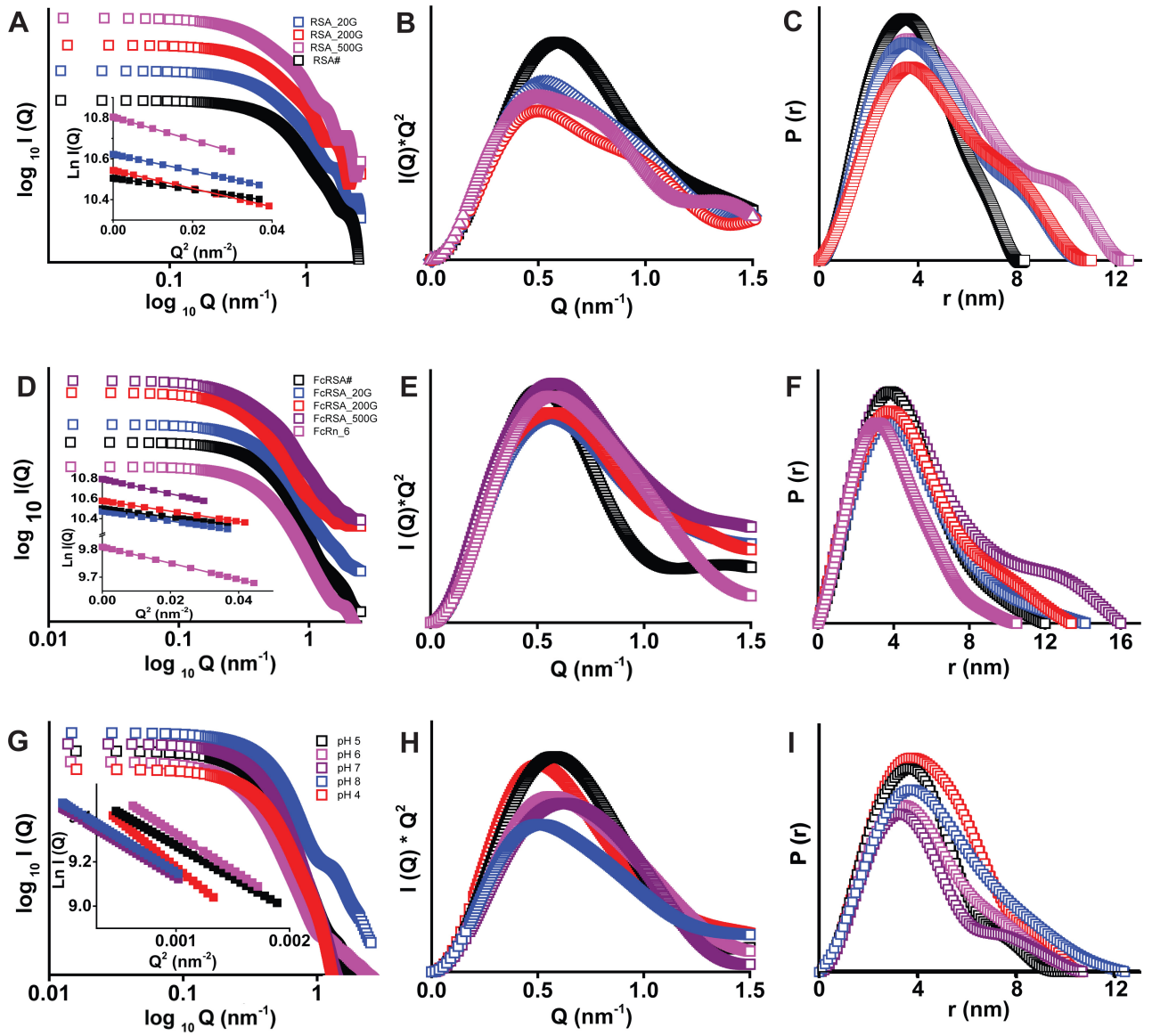

Fig. 5. Small-angle X-ray scattering (SAXS) data analysis from the samples of RSA (*A–C*), RSA-rFcRn (*D–F*), and rFcRn (*G–I*). *A*, *D*, and *G*: SAXS intensity I(Q) profiles of data sets and linear regions of Guinier approximations (*insets*). *B*, *E*, and *H*: Kratky profiles of the data sets. *C*, *F*, and *I*: pairwise distribution function of interatomic vector [P(r)] curves computed from indirect Fourier transformation of measured SAXS data. *Top*, unglycated RSA and its glycated versions [RSA modified with 20, 200, and 500 mM glucose (RSA_20G, RSA_200G, and RSA_500G, respectively)]. *Middle*, rFcRn and its complexes. *Bottom*, plots for rFcRn as a function of pH. I(Q), Kratky, and P(r) plots are arbitrarily translated vertically for clarity.

the pI of albumin more anionic, which may impact albumin interactions.

Altered binding of tagged or modified RSA to FcRn correlates with an increased clearance when examined in the rat. Table 4 shows RSA fluorophore conjugates, their dye-to-RSA ratio, and their respective K_D values at pH 6.0 and 7.4. The conventional conjugation ratio is 4 dyes to 1 albumin molecule; note that most dyes at a >1:1 ratio show reduced binding of RSA to FcRn, as measured with MST. Interestingly, TR sulfonyl chloride, when conjugated at 1:1, had normal binding at pH 6.0 but increased affinity at pH 7.4, whereas TR-X succinimidyl ester at 1:1 and 2:1 behaved like unlabeled RSA with strong binding at pH 6.0 and no binding at pH 7.4. Attachment of the tag at the only reduced thiol of albumin, using maleimide conjugates, also maintained physiological binding characteristics. The modification of albumin-FcRn binding by fluorescent probe conjugation may result from the fluorophore altering key amino acid interactions. Figure 10*A* shows MST analysis of the four fluorescent albumin conjugates that were injected into rats to measure vascular clearance; Fig. 10*B* shows unlabeled RSA and TR-X RSA conjugated 2:1. The direct labeling of RSA with either maleimide or 1:1 TR-X fluorophore resulted in affinity matching previously published results using either Biacore or Isothermal titration calorimetry (4, 10, 58). Note that RSA conjugates with a significantly increased K_D value (TR 4:1 and Alexa 488 4.5:1) were cleared from the plasma of rats more quickly. Figure 10*C* shows the clearance results from rats injected with glycated RSA. Note the striking increase in vascular clear-

Table 3. *Structural parameters of rat FcRn, RSA, and its glycated versions and complexes as deduced from Guinier analysis and indirect Fourier transformation of small-angle X-ray scattering data*

		Guinier Analyses			Indirect Fourier Transformation	
	Concentration, mg/ml	R_g, nm	R_c, nm	L, nm	D_{max}	R_g, nm
Unliganded Protein						
RSA	4.3	2.91	1.79	7.95	8.0	2.89
RSA_20G	4.1	3.48	1.93	10.0	10.0	3.51
RSA_200G	4.4	3.64	1.99	10.5	10.0	3.66
RSA_500G	4.1	4.06	1.96	12.3	12.0	4.13
Protein mixture of rFcRn:RSA (1:1)						
rFcRn_RSA		3.49	1.91	10.12	12.0	3.57
rFcRn_RSA20G		3.68	1.77	11.18	14.1	3.87
rFcRn_RSA_200G		3.83	1.66	11.96	13.4	4.0
rFcRn_RSA500G		4.45	1.74	14.19	16.0	4.78
Unliganded rFcRn						
pH 4	4.3	3.49	2.03	9.83	10.7	3.51
pH 5	4.4	3.0	1.83	8.41	10.3	3.05
pH 6	4.3	3.22	1.8	9.25	10.7	3.33
pH 7	3.8	3.13	1.67	9.17	10.7	3.23
pH 8	3.6	3.56	2.02	10.1	12.4	3.56

RSA, rat serum albumin; RSA_20G, RSA_200G, and RSA_500G are RSA modified with 20, 200, and 500 mM glucose, respectively; R_g, radius of gyration; R_c, radius of cross-section; L, persistant length; D_{max}, maximum linear dimension.

ance for all glycated RSAs, with the most rapid clearance taking place for RSA modified with 500 mM glucose. Since measurement of the different infused albumins is followed by their respective fluorescent tag, we always normalized 2- and 24-h time points to the early time point, <15 min, which is set at 100%. This controls for fluorescent variability and amount of albumin infused in each rat. Since GSC and proximal tubule uptake were normal for glycated albumins, the rapid blood clearance is consistent with the important role of the kidney in reabsorbing filtered physiological albumin for transcytosis and recycling into the circulation, whereas modified albumins with reduced FcRn binding has increased clearance due to lack of reclamation. Figure 11 shows SDS-PAGE gels showing both the Commassie blue

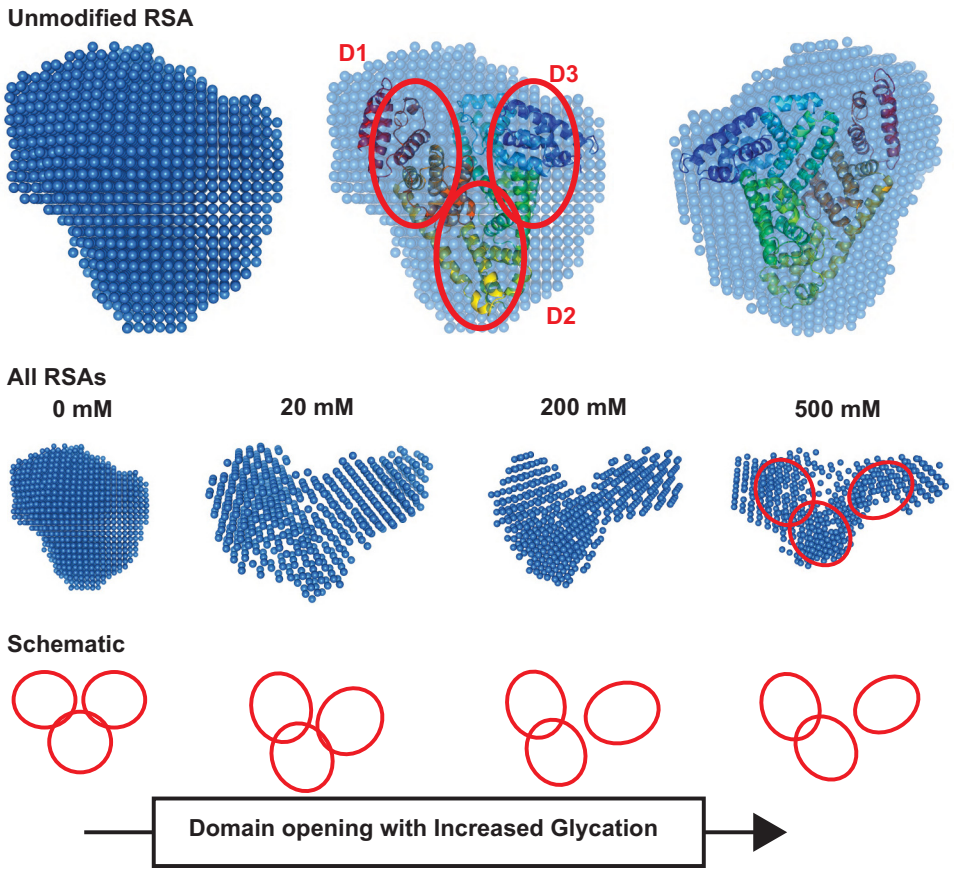

Fig. 6. SAXS density models of RSA. *Top*: SAXS data-based uniform density model of unglycated RSA, its overlay with the crystal structure of ligand-free human serum albumin (Protein Database ID 4K2C), and an orthogonal view of the overlaid SAXS envelope. The red ellipses show the domains of albumin. *Middle*: average uniform density models of glycated versions of RSA. *Bottom*: schematic representation how domain opening and movement lead to shape changes upon increasing glycation.

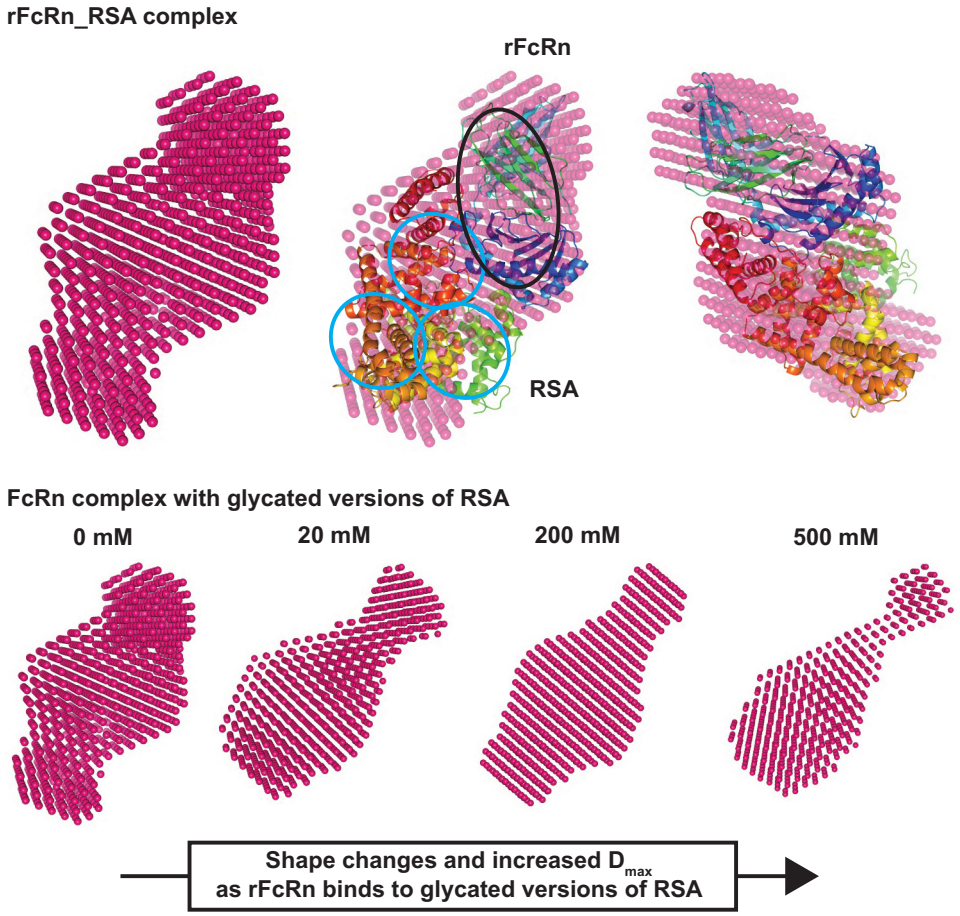

Fig. 7. SAXS density model of glycated RSA-rFcRn. *Top*: SAXS-derived uniform density model of rFcRn and its complex with unglycated RSA, its overlay with the crystal structure of FcRn complexed with human serum albumin (Protein Database ID 4N0F), and orthogonal view of the overlaid SAXS-derived envelope. The black ellipse represents the FcRn receptor associated with β_2-microglobin (β2M), and blue ellipses represent serum albumin. *Bottom*: the complex with unglycated and glycated versions of RSA.

stain and fluorescence in each lane. Figure 11*A* shows blood proteins before and after infusion [early (<15 min), 2 h, and 24 h]. The Commassie blue stain in the control is representative of all Commassie blue-stained gels. The fluorescence shows a protein band with the expected molecular weight of albumin. The clearance is consistent with the fluorescent quantitation shown in Fig. 10, *B* and *C*. To determine whether urine albumin varies when albumins with different FcRn affinities are infused into rats, four rats were infused with control albumin (K_d for FcRn: 2.6 μM) and four rats were infused with modified albumin (K_d for FcRn: >100 μM; Fig. 11*B*). Little intact fluorescent albumin was detected in the urine from rats injected with control albumin. However, when nonbinding or modified albumins were injected, a clear fluorescent albumin band was observed in the urine. This is consistent with a previous report (50) showing that the majority of albumin in urine is degraded.

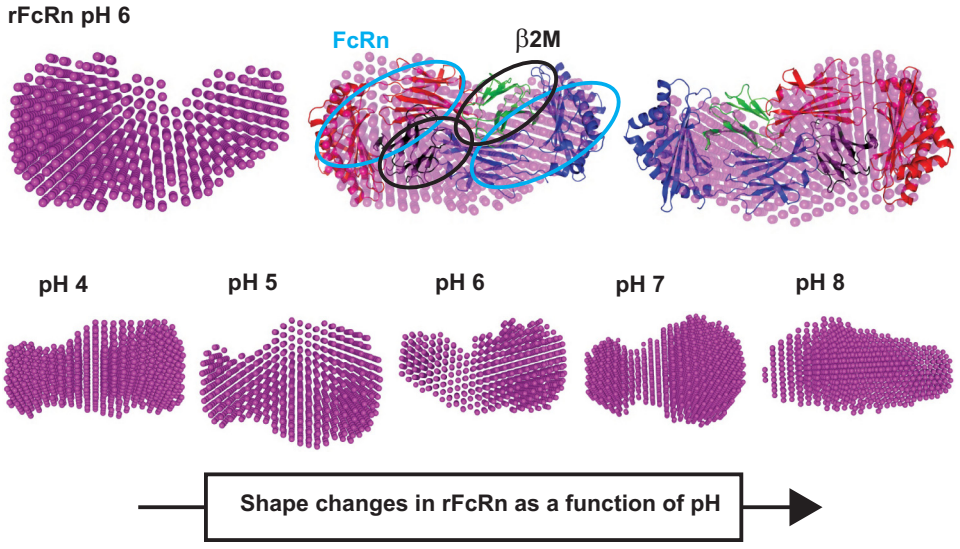

Fig. 8. SAXS density model of rFcRn and effect of pH. *Top*: SAXS data-based uniform density model of rFcRn at pH 6, its overlay with the crystal structure of heterodimer FcRn (Protein Database ID 3FRU), and two different views. The light blue ellipses represent the Fc receptor, and the black ellipses show the presence of β2M. *Bottom*: uniform density models obtained as a function of varying buffer pH 4–8.

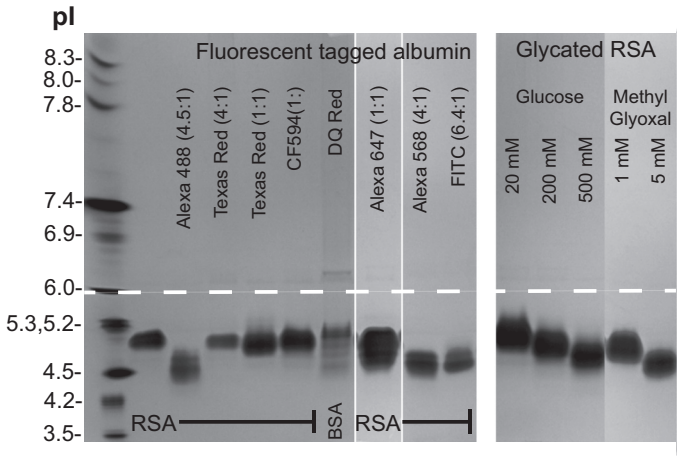

Fig. 9. Evaluation of albumin pI after fluorophore conjugation and glycation. Modified albumins were separated on a 3–10 isoelectric focusing (IEF) protein gel along with IEF markers pI 3.5–10. *Left*: fluorophore-conjugated albumins with Alexa 488, Alexa 568, and FITC showing a charge shift to a more anionic form. DQ red BSA, which is highly conjugated with Bodipy Texas red-X, results in multiple bands. *Right*: glycated albumins showing concentration-dependent decreases in pI, with 5 mM methylgloxal resulting in the largest charge shift.

DISCUSSION

The clinical importance of albumin and the role of the kidney in its long plasma half-life is well understood (14). Thus, understanding the reabsorption requirements of glomerular filtered albumin and how it is processed for either degradation or transcytosis by proximal tubule cells is an area of active investigation (7, 14, 35, 70). The present study focused on defining, in more detail, the interaction of rat FcRn with rat albumin. This is important since the kidney disease model best suited for intravital microscopy is the MWF rat model, which enables visualization of both glomerular filtration and proximal tubule uptake of filtered molecules.

FcRn-albumin. Since previous studies have documented affinity differences between FcRn and albumins from multiple species, our first step involved examining rat FcRn binding to albumins of different species. To establish that MST is a reproducible and valid method to look at this interaction, binding of rat FcRn to rat albumin and rat IgG was determined. Figure 2, *A* and *B*, show that, using this method, FcRn does exhibit pH-sensitive binding to both albumin and IgG with the observed K_D values in agreement with previous studies. To address species differences, we determined K_D values for seven different albumins and four IgGs (Fig. 3, *A* and *B*, and Table 1). Only rat and rabbit albumin displayed pH-sensitive binding with other albumins, showing weak binding at both pHs. Similarly, rabbit IgG was the only IgG that showed an affinity similar to rat IgG. Interestingly, bovine IgG had a high affinity at both pHs, whereas mouse IgG showed weak binding at both. Differences in the pH affinity if albumin are likely to alter its normal intracellular trafficking. Proteins that have increased affinity at both pHs would be expected to have shorter half-lives since the normal pH-sensitive steps would be inhibited and reclamation via transcytosis reduced. Consequently, it is important for in vivo studies to understand how albumin probes interact with the endogenous receptor. At a minimum, one must be cautious of interpreting results when the affinity has not been determined.

Albumin alteration in disease, impact on interaction with FcRn, and proximal tubule cell injury. Over 30 yr ago, glucosylated albumin was found to be present in normal human serum and increased in diabetes (13, 19). Soon afterward, it was reported that glucosylated albumin was handled differently than unmodified albumin, leading to the editing hypothesis, which proposed selective filtration and excretion of glucosylated albumin (17, 29, 30). This editing process was reduced in diabetic animals, and it was proposed that the proximal tubule may be the site of editing and that normal editing returned if blood glucose levels were controlled (29). Diabetes, aging, and other factor known to alter albumin may alter its interaction with renal proximal tubules independent of glomerular changes (9, 31, 49, 74). More recent data using the rat streptozotocin diabetes model showed no significant change in glomerular filtration but a significant decrease in albumin uptake by proximal tubules, supporting earlier studies that predicted that editing was done in the proximal tubule (50, 71). In the present study, evaluation of glycated albumin filtration and proximal tubule uptake was first performed to determine whether in a healthy animal any alteration in its handling was occurring. As shown in Fig. 1, no significant changes in proximal tubule uptake were observed, suggesting a more distal event, i.e., proximal tubule processing of albumin was altered. Both cubilin/megalin receptor-mediated uptake and fluid phase uptake pathways could be participating in glycated albumin uptake, and any impact of glycated albumin on these pathways requires further investigation. However, to address whether the interaction of glycated albumin with FcRn is altered, both human and rat albumins were evaluated. Both glucose and MGO-modified albumins had significant decreased affinity for FcRn (Fig. 4, *A–D*). This would prevent these albumins from being transcytosed. Abnormal protein delivery to the proximal tubule has been shown to activate multiple phenotypic changes, including complement and inflammasome activation and au-

Table 4. *Assessment of fluorescent dye albumin conjugates on FcRn binding using MST analysis*

Fluorophore Conjugate (Ratio of Dye to Albumin)	pH 6 K_D, μM)	pH 7.4 K_D, μM
CF-594 maleimide*		
1:3	1.5	NB
Texas red-X*		
1:1	5.4	NB
Texas red*		
4:1	>40	NB
Alexa 488*		
4.5:1	NB	NB
Fluorescein		
6.4:1	69	1.0
Alexa 568		
4:1	17	NB
Texas red-X		
2:1	10	NB
Texas red-X		
5:1	>100	NB
Texas red		
1:1	6	11
Alexa 647 maleimide		
1:1	11	NB
DQ BSA	NB	NB
No dye	11.6	>100

*Data from present study.

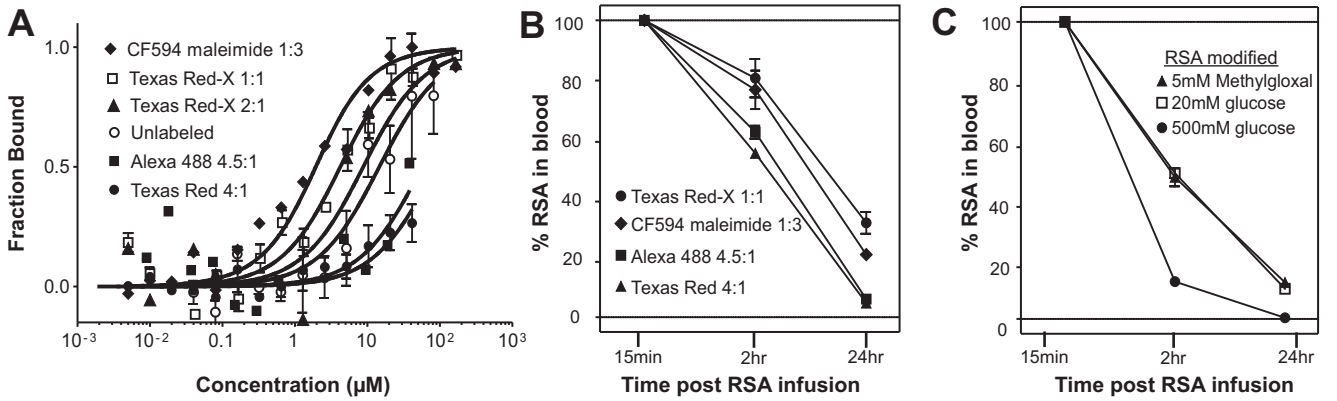

Fig. 10. Fluorophore conjugation of albumin can alter FcRn binding and the rate of vascular clearance. Rat albumin was conjugated to multiple fluorophores at different ratios, and binding to FcRn was evaluated with MST at pH 6.0 (*A*). An increased conjugation ratio of dye to protein resulted in decreased binding. Table 4 shows all dye-albumin conjugates examined and their affinity at pH 6.0 and 7.4. To address whether decreased binding to FcRn correlated with vascular clearance increase, we infused the four conjugates shown into rats and collected blood over a 24-h time period ($n = 3$). The 15-min collection time point was set to 100%, and the decrease in fluorescence was followed at 2 and 24 h. *B*: percent tagged albumin in blood at 2 and 24 h. Note that clearance was faster for albumins with decreased binding to FcRn. To address the clearance of glycated albumin, rats were infused with both methylgloxal- and glucose-modified RSA. Clearance was again increased, most dramatically for the 500 mM glucose-modified albumin (*C*).

tophagy (33, 77). This cascade of events initiated by increased delivery to and mishandling of proteins by the proximal tubule is known to result in kidney injury.

One possible explanation for the altered binding of modified albumin to FcRn was that glycation altered the normal structure of albumin (6, 45). Previous examination of glycated albumin using fluorescence (61), Fourier transformed infrared (12), circular dichroism and microviscometer (57), and assorted spectroscopic methods (24) all confirmed that glycated albumin had significantly decreased α-helical and increased β-sheet structure compared with nonmodified albumin. To extend these findings as well as to examine the interaction of FcRn with albumin, SAXS analysis was conducted (59). Increasing concentrations of glucose increased the R_g and D_{max} values of albumin (Fig. 5 and 6 and Table 3). FcRn (Figs. 7 and 8 and Table 3) did not show significant structural changes between pH 6 and 7; however, changes were noticed at more basic and acidic pHs. When FcRn and the glycated albumins were incubated together to carry out binding experiments and SAXS was performed, both Guinier and Autognom analyses showed significant changes in shape, which increased with increasing glycation (Fig. 7 and Table 3). However, the exact organization of glycated albumins was unclear since the crystal structure is unavailable for glycated albumin and the data were fit using unglycated albumin. Our SAXS data-based models provide visual insights that with the increase in glycation, the domains of RSA progressively open away from each other. Previous studies using amino acid analysis, mass spectrometry methods, and molecular modeling found preferred lysine residues for glycation (23, 32, 48). Most preferred sites are in

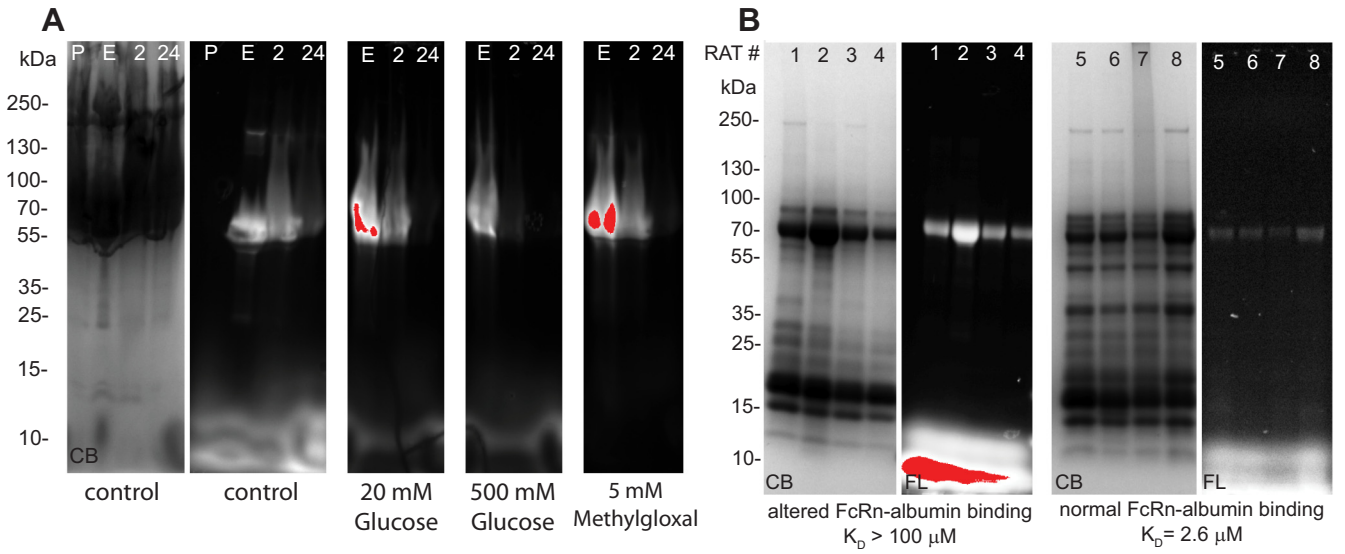

Fig. 11. Presence of control and modified albumin in blood and urine after infusion. Rat albumin was infused into rats, and blood and urine samples were collected and analyzed by SDS-PAGE. Gels were imaged for fluorescence and stained for total protein using Coomassie blue stain. *A*: blood samples quantitated in Fig. 10*C* showing the more rapid vascular clearance of the modified albumins. P, preinfusion; E, early (<15 min). Note that 500 mM glucose-modified albumin had the most rapid clearance. *B*: 24-h urine from 8 rats was analyzed. *Rats 1–4* received modified albumin and *rats 5–8* received control albumin. Note the increased presence of intact albumin in rats that received albumin with decreased FcRn binding.

albumin DII and DIII, with 33% of overall glycation occurring at Lys^{525} in albumin DIII. In addition, Lys^{573}, which is unique to humans, is essential to interact with β_2-microglobin by forming interfacial salt bridges with Glu^{69} (41). Previous studies have suggested that the attached light chain is essential for interactions with albumin, and glycation at Lys^{573} may reduce its interactions with the light chain of the neonatal receptor, which, in turn, reduces its affinity with serum albumin. Multiple sequence alignment showed the importance of conserved lysine residues in serum albumins of different species in the context of glycation, which also provide the reason for the higher binding affinity of the human serum albumin K573P mutant. These results, along with our observations, suggest that the openings we observed in our models are due to glycation in albumin DII and DIII. However, a recent report (52) has also showed that both ablumin DI and DIII are required for optimal pH-dependent binding to FcRn. Given these restrictions, it is still very clear that the glycation of albumin does alter its structure. This, combined with our binding data, supports that glycation through steric hindrance and/or modifications of key amino acids alter the normal FcRn-albumin binding site. Additional work is underway to determine how these modifications impact the interaction of albumin with cubilin, which may, in conjunction with megalin, be responsible for the significant albumin uptake in proximal tubule cells (1, 14). The pharmacokinetics of albumin and the impact of glycosylation have been previously reported, but this is the first report to address the mechanism (6). Given the multitude of modifications and associations that albumin undergoes, many correlate with disease processes, and deciphering how these "different" albumins bind to their receptors becomes critical for defining and eventually manipulating the uptake, transport, and recycling of albumin and its cargo.

Two-photon imaging and modified albumin. The advent of two-photon intravital microscopy has enabled multiple novel studies that have revealed and clarified existing and new cell dynamics in many tissues and organisms. We have used this technology to investigate kidney dynamics and, in particular, the glomerular filtration and proximal tubule reabsorption of albumin. One requirement of these studies is that tracer amounts of albumin are tagged with a fluorescent probe enabling real-time visualization of its movement. While this approach is commonplace in fluorescent studies, assessment of the impact of the tag on the molecule's normal interactions is often not addressed. Therefore, we evaluated multiple fluorescent tags, at different conjugation ratios, and determined their effect on FcRn binding. Since charge has been shown to be a potential modifier of albumin's interactions, we first examined some of the conjugates using IEF. Figure 9 (25, 62) shows that glycated and some fluorescent tagged rat albumins became slightly more anionic. TR, CF-594, and Alexa 647 fluorophores did not alter the pI of albumin, whereas DQ albumin was composed of multiple charged species. The placement and type of conjugation are clearly important, as seen with TR albumin, since the TR-X (contains spacer), even at a 2:1 conjugation, retained normal pH-dependent interactions with FcRn, whereas TR lacking the spacer showed abnormal pH-dependent binding even at a 1:1 conjugation (Fig. 10*A* and Table 4). Since there were clear differences in FcRn affinity, we predicted their serum clearance would correlate with binding differences. We found that those with normal pH-dependent binding were recycled and had the slowest vascular clearance, whereas those with decreased binding were cleared more rapidly from the plasma. The results shown in Fig. 10*B* confirmed that the TR and Alexa 488 albumin conjugates were cleared more rapidly than TR-X and CF-594 albumin conjugates. Given these results, and the fact that FcRn has species-specific variations, in vivo studies exploring the handling of albumin need to be cautious with their interpretations, especially if they have not determined how their albumin probe interacts with FcRn. An effective tracer molecule for albumin requires characterization since correct interpretation of in vitro and in vivo studies requires physiological behavior. A decrease in binding affinity between FcRn and albumin at low pH would inhibit its transcytosis, resulting in more albumin being transported to the degradative pathway via cubilin/megalin (14, 43). In addition, a lack of a reduction in binding at a higher pH may lead to the accumulation of the fluorescent albumin tracer within proximal tubule cells. Since we found that the proximal tubule uptake of glycated albumin (Fig. 1) was normal, the uptake pathways (cubilin/megalin and fluid phase endocytosis) are functional. Determining whether glycated albumin alters these pathways differently and/or whether extended exposure to glycated albumin changes the dynamics are important questions. Additional support for the importance of FcRn-albumin interactions was obtained when glycated albumins were evaluated for vascular clearance (Fig. 10C). Again, note the more rapid clearance in albumin that has reduced affinity for FcRn. These data are consistent with our hypothesis that reduced transcytosis mediated by reduced albumin-FcRn binding enabled intracellular molecular sorting and catabolism of chemically modified albumin, which is then released into the proximal tubule lumen and excreted (14). Consistent with this hypothesis is the increased of non-FcRn-binding albumin in the urine (Fig. 11*B*).

In conclusion, we report that glycated albumin has a normal glomerular filtration rate and normal proximal tubule uptake but altered binding to the only known albumin transcytotic receptor, FcRn. Furthermore, we propose that structural changes induced by glycation account for the reduced affinity with FcRn and that this, in turn, reduces transcytosis and increases intracellular catabolism, resulting in the excretion of albumin fragments and more rapid vascular clearance. In addition, while fluorescent conjugated probes are very valuable research tools, we documented significant variability in the binding affinity of albumin conjugates to FcRn dependent on the conjugation ratio and probe. This highlights the importance of characterizing the impact of molecular tags on protein-protein interactions since these can impact in vivo interactions and consequently alter the normal trafficking of a protein, as observed in fluorescence microscopy studies.

ACKNOWLEDGMENTS

Authors also acknowledge the Council of Scientific and Industrial Research Institute of Microbial Technology in-house SAXS facility for SAXS data collection.

Present address of M. Patel: Providence Health and Services, Portland, OR 97213.

Present address of B. Flores: University Michigan Graduate Program in Cellular and Molecular Biology, Ann Arbor, MI 48109.

GRANTS

This work was supported by National Institute of Diabetes and Digestive and Kidney Diseases Grants DK-091623 and DK-079312 (to B. A. Molitoris) and a Veterans Administration merit review award. S. Pratap is the recipient of a DST Inspire Research fellowship.

DISCLOSURES

No conflicts of interest, financial or otherwise, are declared by the author(s).

AUTHOR CONTRIBUTIONS

Author contributions: M.C.W., A.A., and B.A.M. conception and design of research; M.C.W., J.M., S.P., B.F., G.J.R., R.S., S.K., and M.P. performed experiments; M.C.W., J.M., S.P., R.S., M.P., A.A., and B.A.M. analyzed data; M.C.W., S.P., R.S., M.P., A.A., and B.A.M. interpreted results of experiments; M.C.W., S.P., R.S., and A.A. prepared figures; M.C.W., A.A., and B.A.M. drafted manuscript; M.C.W., S.P., A.A., and B.A.M. edited and revised manuscript; M.C.W., A.A., and B.A.M. approved final version of manuscript.

REFERENCES

1. **Amsellem S, Gburek J, Hamard G, Nielsen R, Willnow TE, Devuyst O, Nexo E, Verroust PJ, Christensen EI, Kozyraki R.** Cubilin is essential for albumin reabsorption in the renal proximal tubule. *J Am Soc Nephrol* 21: 1859–67, 2010.
2. **Andersen JT, Cameron J, Plumridge A, Evans L, Sleep D, Sandlie I.** Single-chain variable fragment albumin fusions bind the neonatal Fc receptor (FcRn) in a species-dependent manner: implications for in vivo half-life evaluation of albumin fusion therapeutics. *J Biol Chem* 288: 24277–24285, 2013.
3. **Andersen JT, Daba MB, Berntzen G, Michaelsen TE, Sandlie I.** Cross-species binding analyses of mouse and human neonatal Fc receptor show dramatic differences in immunoglobulin G and albumin binding. *J Biol Chem* 285: 4826–36, 2010.
4. **Andersen JT, Dalhus B, Cameron J, Daba MB, Plumridge A, Evans L, Brennan SO, Gunnarsen KS, Bjørås M, Sleep D, Sandlie I.** Structure-based mutagenesis reveals the albumin-binding site of the neonatal Fc receptor. *Nat Commun* 3: 610, 2012.
5. **Andersen JT, Dee Qian J, Sandlie I.** The conserved histidine 166 residue of the human neonatal Fc receptor heavy chain is critical for the pH-dependent binding to albumin. *Eur J Immunol* 36: 3044–3051, 2006.
6. **Anguizola J, Matsuda R, Barnaby OS, Hoy KS, Wa C, DeBolt E, Koke M, Hage DS.** Review: Glycation of human serum albumin. *Clin Chim Acta* 425: 64–76, 2013.
7. **Birn H, Christensen EI.** Renal albumin absorption in physiology and pathology. *Kidney Int* 69: 440–449, 2006.
8. **Bohlender JM, Franke S, Stein G, Wolf G.** Advanced glycation end products and the kidney. *Am J Physiol Renal Physiol* 289: F645–F659, 2005.
9. **Cessac AL, Perichon M, Schaeverbeke J, Bakala H.** Age-related changes in albumin binding by renal brush-border membrane vesicles. *Mech Ageing Dev* 70: 139–148, 1993.
10. **Chaudhury C, Brooks CL, Carter DC, Robinson JM, Anderson CL.** Albumin binding to FcRn: distinct from the FcRn-IgG interaction. *Biochemistry* 45: 4983–4990, 2006.
11. **Chaudhury C, Mehnaz S, Robinson JM, Hayton WL, Pearl DK, Roopenian DC, Anderson CL.** The major histocompatibility complex-related Fc receptor for IgG (FcRn) binds albumin and prolongs its lifespan. *J Exp Med* 197: 315–322, 2003.
12. **Chesne S, Rondeau P, Armenta S, Bourdon E.** Effects of oxidative modifications induced by the glycation of bovine serum albumin on its structure and on cultured adipose cells. *Biochimie* 88: 1467–77, 2006.
13. **Day JF, Thorpe SR, Baynes JW.** Nonenzymatically glucosylated albumin. In vitro preparation and isolation from normal human serum. *J Biol Chem* 254: 595–597, 1979.
14. **Dickson LE, Wagner MC, Sandoval RM, Molitoris BA.** The proximal tubule and albuminuria: really! *J Am Soc Nephrol* 25: 443–53, 2014.
15. **Firan M, Bawdon R, Radu C, Ober RJ, Eaken D, Antohe F, Ghetie V, Ward ES.** The MHC class I-related receptor, FcRn, plays an essential role in the maternofetal transfer of gamma-globulin in humans. *Int Immunol* 13: 993–1002, 2001.
16. **Gastinel LN, Simister NE, Bjorkman PJ.** Expression and crystallization of a soluble and functional form of an Fc receptor related to class I histocompatibility molecules. *Proc Natl Acad Sci USA* 89: 638–642, 1992.
17. **Ghiggeri GM, Candiano G, Delfino G, Bianchini F, Queirolo C.** Glycosyl albumin and diabetic microalbuminuria: demonstration of an altered renal handling. *Kidney Int* 25: 565–570, 1984.
18. **Goebl NA, Babbey CM, Datta-Mannan A, Witcher DR, Wroblewski VJ, Dunn KW.** Neonatal Fc receptor mediates internalization of Fc in transfected human endothelial cells. *Mol Biol Cell* 19: 5490–5505, 2008.
19. **Guthrow CE, Morris MA, Day JF, Thorpe SR, Baynes JW.** Enhanced nonenzymatic glucosylation of human serum albumin in diabetes mellitus. *Proc Natl Acad Sci USA* 76: 4258–4261, 1979.
20. **Haymann JP, Levraud JP, Bouet S, Kappes V, Hagege J, Nguyen G, Xu Y, Rondeau E, Sraer JD.** Characterization and localization of the neonatal Fc receptor in adult human kidney. *J Am Soc Nephrol* 11: 632–639, 2000.
21. **He W, Ladinsky MS, Huey-Tubman KE, Jensen GJ, McIntosh JR, Bjorkman PJ, He W, Ladinsky MS, Huey-Tubman KE, Jensen GJ, McIntosh JR, Bjorkman PJ.** FcRn-mediated antibody transport across epithelial cells revealed by electron tomography. *Nature* 455: 542–546, 2008.
22. **Huber AH, Kelley RF, Gastinel LN, Bjorkman PJ.** Crystallization and stoichiometry of binding of a complex between a rat intestinal Fc receptor and Fc. *J Mol Biol* 230: 1077–1083, 1993.
23. **Iberg N, Fluckiger R.** Nonenzymatic glycosylation of albumin in vivo. Identification of multiple glycosylated sites. *J Biol Chem* 261: 13542–13545, 1986.
24. **Indurthi VS, Leclerc E, Vetter SW.** Interaction between glycated serum albumin and AGE-receptors depends on structural changes and the glycation reagent. *Arch Biochem Biophys* 528: 185–196, 2012.
25. **Iwao Y, Hiraike M, Kragh-Hansen U, Mera K, Noguchi T, Anraku M, Kawai K, Maruyama T, Otagiri M.** Changes of net charge and α-helical content affect the pharmacokinetic properties of human serum albumin. *Biochim Biophys Acta* 1774: 1582–1590, 2007.
26. **Jerabek-Willemsen M, André T, Wanner R, Roth HM, Duhr S, Baaske P, Breitsprecher D.** Microscale thermophoresis: interaction analysis and beyond. *J Mol Struct* 1077: 101–113, 2014.
27. **Kim J, Bronson CL, Hayton WL, Radmacher MD, Roopenian DC, Robinson JM, Anderson CL.** Albumin turnover: FcRn-mediated recycling saves as much albumin from degradation as the liver produces. *Am J Physiol Gastrointest Liver Physiol* 290: G352–G360, 2006.
28. **Konarev PV, Volkov VV, Sokolova AV, Koch MH, Svergun DI.** PRIMUS: a Windows PC-based system for small-angle scattering data analysis. *J Appl Crystallogr* 36: 1277–1282, 2003.
29. **Kowluru A, Kowluru BYA, Kowluru R, Bitensky MW, Corwin EJ, Solomon SS, Johnson JD.** Suggested mechanism for the selective excretion of glucosylated albumin. the effects of diabetes mellitus and aging on this process and the origins of diabetic microalbuminuria mellitus and include microscopic albuminuria. *J Exp Med* 166: 1259–1279, 1987.
30. **Kowluru A, Kowluru RA, Solomon S, Martinez L.** Protein glycation: Effects upon protein recognition by the proximal tubule. *Life Sci* 50: 281–286, 1992.
31. **Kunika K, Yamaoka T, Itakura M.** Diabetic damage of selective renal reabsorption assessed by albumin negative charge. *Diabetes Res Clin Pract* 33: 181–189, 1996.
32. **Lapolla A, Fedele D, Reitano R, Aricò NC, Seraglia R, Traldi P, Marotta E, Tonani R.** Enzymatic digestion and mass spectrometry in the study of advanced glycation end products/peptides. *J Am Soc Mass Spectrom* 15: 496–509, 2004.
33. **Levey AS, Becker C, Inker LA.** Glomerular filtration rate and albuminuria for detection and staging of acute and chronic kidney disease in adults: a systematic review. *JAMA* 313: 837–846, 2015.
34. **Medesan C, Cianga P, Mummert M, Stanescu D, Ghetie V, Ward ES.** Comparative studies of rat IgG to further delineate the Fc:FcRn interaction site. *Eur J Immunol* 28: 2092–2100, 1998.
35. **Merlot AM, Kalinowski DS, Richardson DR.** Unraveling the mysteries of serum albumin-more than just a serum protein. *Front Physiol* 5: 299, 2014.
36. **Neuber T, Frese K, Jaehrling J, Jäger S, Daubert D, Felderer K, Linnemann M, Höhne A, Kaden S, Kölln J, Tiller T, Brocks B, Ostendorp R, Pabst S.** Characterization and screening of IgG binding to the neonatal Fc receptor. *MAbs* 6: 928–942, 2014.
37. **Ober RJ, Martinez C, Vaccaro C, Zhou J, Ward ES, Ober RJ, Martinez C, Vaccaro C, Zhou J, Ward ES.** Visualizing the site and dynamics of IgG salvage by the MHC class I-related receptor, FcRn. *J Immunol* 172: 2021–2029, 2004.

38. **Ober RJ.** Differences in promiscuity for antibody-FcRn interactions across species: implications for therapeutic antibodies. *Int Immunol* 13: 1551–1559, 2001.
39. **Peters TJ.** *All About Albumin Biochemistry, Genetics, and Medical Applications*. New York: Academic, 1996.
40. **Petoukhov MV, Franke D, Shkumatov AV, Tria G, Kikhney AG, Gajda M, Gorba C, Mertens HD, Konarev PV, Svergun DI.** New developments in the ATSAS program package for small-angle scattering data analysis. *J Appl Crystallogr* 45: 342–350, 2012.
41. **Plumridge A, Sleep D, Cameron J, Sandlie I, Andersen JT, Friis EP.** *Google Patents. Albumin Variants* (online). http://www.google.com/patents/US8748380 [16 March 2016].
42. **Prabhat P, Gan Z, Chao J, Ram S, Vaccaro C, Gibbons S, Ober RJ, Ward ES, Prabhat P, Gan Z, Chao J, Ram S, Vaccaro C, Gibbons S, Ober RJ, Ward ES.** Elucidation of intracellular recycling pathways leading to exocytosis of the Fc receptor, FcRn, by using multifocal plane microscopy. *Proc Natl Acad Sci USA* 104: 5889–5894, 2007.
43. **Pyzik M, Rath T, Lencer WI, Baker K, Blumberg RS.** FcRn: the architect behind the immune and nonimmune functions of IgG and albumin. *J Immunol* 194: 4595–4603, 2015.
44. **Quinlan GJ, Martin GS, Evans TW.** Albumin: biochemical properties and therapeutic potential. *Hepatology* 41: 1211–1219, 2005.
45. **Raghav A, Ahmad J.** Glycated serum albumin: a potential disease marker and an intermediate index of diabetes control. *Diabetes Metab Syndr* 8: 245–251, 2014.
46. **Rambo RP, Tainer JA.** Accurate assessment of mass, models and resolution by small-angle scattering. *Nature* 496: 477–481, 2013.
47. **Roche M, Rondeau P, Singh NR, Tarnus E, Bourdon E.** The antioxidant properties of serum albumin. *FEBS Lett* 582: 1783–1787, 2008.
48. **Rondeau P, Bourdon E.** The glycation of albumin: structural and functional impacts. *Biochimie* 93: 645–658, 2011.
49. **Russo LM, Osicka TM, Brammar GC, Candido R, Jerums G, Comper WD.** Renal processing of albumin in diabetes and hypertension in rats. *Am J Nephrol* 23: 61–70, 2003.
50. **Russo LM, Sandoval RM, Campos SB, Molitoris BA, Comper WD, Brown D.** Impaired tubular uptake explains albuminuria in early diabetic nephropathy. *J Am Soc Nephrol* 20: 489–494, 2009.
51. **Russo LM, Sandoval RM, McKee M, Osicka TM, Collins AB, Brown D, Molitoris BA, Comper WD.** The normal kidney filters nephrotic levels of albumin retrieved by proximal tubule cells: retrieval is disrupted in nephrotic states. *Kidney Int* 71: 504–513, 2007.
52. **Sand KM, Bern M, Nilsen J, Dalhus B, Gunnarsen KS, Cameron J, Grevys A, Bunting K, Sandlie I, Andersen JT.** Interaction with both domain I and III of albumin is required for optimal pH dependent binding to the neonatal Fc receptor (FcRn). *J Biol Chem* 289: 34583–34594, 2014.
53. **Sand KM, Bern M, Nilsen J, Noordzij HT, Sandlie I, Andersen JT.** Unraveling the Interaction between FcRn and albumin: opportunities for design of albumin-based therapeutics. *Front Immunol* 5: 1–21, 2015.
54. **Sandoval RM, Molitoris BA.** Quantifying endocytosis in vivo using intravital two-photon microscopy. *Methods Mol Biol* 440: 389–402, 2008.
55. **Sandoval RM, Wagner MC, Patel M, Campos-Bilderback SB, Rhodes GJ, Wang E, Wean SE, Clendenon SS, Molitoris a B.** Multiple factors influence glomerular albumin permeability in rats. *J Am Soc Nephrol* 23: 447–457, 2012.
56. **Sarav M, Wang Y, Hack BK, Chang A, Jensen M, Bao L, Quigg RJ.** Renal FcRn reclaims albumin but facilitates elimination of IgG. *J Am Soc Nephrol* 20: 1941–1952, 2009.
57. **Sattarahmady N, Moosavi-Movahedi AA, Ahmad F, Hakimelahi GH, Habibi-Rezaei M, Saboury AA, Sheibani N.** Formation of the molten globule-like state during prolonged glycation of human serum albumin. *Biochim Biophys Acta* 1770: 933–42, 2007.
58. **Schmidt MM, Townson SA, Andreucci AJ, King BM, Schirmer EB, Murillo AJ, Dombrowski C, Tisdale AW, Lowden PA, Masci AL, Kovalchin JT, Erbe DV, Wittrup KD, Furfine ES, Barnes TM.** Crystal structure of an HSA/FcRn complex reveals recycling by competitive mimicry of HSA ligands at a pH-dependent hydrophobic interface. *Structure* 21: 1966–1978, 2013.
59. **Schneidman-Duhovny D, Kim SJ, Sali A.** Integrative structural modeling with small angle X-ray scattering profiles. *BMC Struct Biol* 12: 17, 2012.
60. **Seidel SAI, Dijkman PM, Lea WA, van den Bogaart G, Jerabek-Willemsen M, Lazic A, Joseph JS, Srinivasan P, Baaske P, Simeonov A, Katritch I, Melo FA, Ladbury JE, Schreiber G, Watts A, Braun D, Duhr S.** Microscale thermophoresis quantifies biomolecular interactions under previously challenging conditions. *Methods* 59: 301–315, 2013.
61. **Shaklai N, Garlick RL, Bunn HF.** Nonenzymatic glycosylation of human serum albumin alters its conformation and function. *J Biol Chem* 259: 3812–3817, 1984.
62. **Smith KR, Borchardt RT.** Permeability and mechanism of albumin, cationized albumin, and glycosylated albumin transcellular transport across monolayers of cultured bovine brain capillary endothelial cells. *Pharm Res* 6: 466–473, 1989.
63. **Solanki AK, Rathore YS, Badmalia MD, Dhoke RR, Nath SK, Nihalani D, Ashish.** Global shape and ligand binding efficiency of the HIV-1-neutralizing antibodies differ from those of antibodies that cannot neutralize HIV-1. *J Biol Chem* 289: 34780–34800, 2014.
64. **Svergun D, Barberato C, Koch MH.** CRYSOL: a program to evaluate X-ray solution scattering of biological macromolecules from atomic coordinates. *J Appl Crystallogr* 28: 768–773, 1995.
65. **Svergun DI, Petoukhov MV, Koch MH.** Determination of domain structure of proteins from X-ray solution scattering. *Biophys J* 80: 2946–2953, 2001.
66. **Svergun DI.** Determination of the regularization parameter in indirect-transform methods using perceptual criteria. *J Appl Crystallogr* 25: 495–503, 1992.
67. **Svergun DI.** Restoring low resolution structure of biological macromolecules from solution scattering using simulated annealing. *Biophys J* 76: 2879–2886, 1999.
68. **Tenten V, Menzel S, Kunter U, Sicking EM, van Roeyen CRC, Sanden SK, Kaldenbach M, Boor P, Fuss A, Uhlig S, Lanzmich R, Willemsen B, Dijkman H, Grepl M, Wild K, Kriz W, Smeets B, Floege J, Moeller MJ.** Albumin is recycled from the primary urine by tubular transcytosis. *J Am Soc Nephrol* 24: 1966–1980, 2013.
69. **Tesar DB, Björkman PJ.** An intracellular traffic jam: Fc receptor-mediated transport of immunoglobulin G. *Curr Opin Struct Biol* 20: 226–233, 2010.
70. **Tojo A, Kinugasa S.** Mechanisms of glomerular albumin filtration and tubular reabsorption. *Int J Nephrol* 2012: 481520, 2012.
71. **Tojo A, Onozato ML, Ha H, Kurihara H, Sakai T, Goto A, Fujita T, Endou H.** Reduced albumin reabsorption in the proximal tubule of early-stage diabetic rats. *Histochem Cell Biol* 116: 269–276, 2001.
72. **Vaughn DE, Bjorkman PJ.** High-affinity binding of the neonatal Fc receptor to its IgG ligand requires receptor immobilization. *Biochemistry* 36: 9374–9380, 1997.
73. **Vaughn DE, Bjorkman PJ.** Structural basis of pH-dependent antibody binding by the neonatal Fc receptor. *Structure* 6: 63–73, 1998.
74. **Verbeke P, Perichon M, Schaeverbeke J, Bakala H.** Effect of glycation of albumin on its binding to renal brush-border membrane vesicles: influence of aging in rats. *Biochim Biophys Acta Biomembr* 1282: 93–100, 1996.
75. **West AP, Bjorkman PJ.** Crystal structure and immunoglobulin G binding properties of the human major histocompatibility complex-related Fc receptor. *Biochemistry* 39: 9698–9708, 2000.
76. **Zhou J, Johnson JE, Ghetie V, Ober RJ, Ward ES.** Generation of mutated variants of the human form of the MHC class i-related receptor, FcRn, with increased affinity for mouse immunoglobulin G. *J Mol Biol* 332: 901–913, 2003.
77. **Zoja C, Abbate M, Remuzzi G.** Progression of renal injury toward interstitial inflammation and glomerular sclerosis is dependent on abnormal protein filtration. *Nephrol Dial Transplant* 30: 706–712, 2014.